IOP Publishing Journal of Physics B: Atomic, Molecular and Optical Physics

J. Phys. B: At. Mol. Opt. Phys. **49** (2016) 234001 (9pp) doi:10.1088/0953-4075/49/23/234001

Stereochemical configuration and selective excitation of the chiral molecule halothane

Martin Pitzer[1,2,5], Gregor Kastirke[1], Phillip Burzynski[1], Miriam Weller[1], Daniel Metz[1], Jonathan Neff[1], Markus Waitz[1], Florian Trinter[1], Lothar Ph H Schmidt[1], Joshua B Williams[3], Till Jahnke[1], Horst Schmidt-Böcking[1], Robert Berger[4], Reinhard Dörner[1] and Markus Schöffler[1]

[1] Institute for Nuclear Physics, Johann Wolfgang Goethe-University Frankfurt, Max-von-Laue-Straße 1, D-60438 Frankfurt, Germany
[2] Experimental Physics IV, University of Kassel, Heinrich-Plett-Straße 40, D-34132 Kassel, Germany
[3] Department of Physics, University of Nevada, Reno, 1664 N. Virginia Street, Reno, NV 89557, USA
[4] Fachbereich Chemie, Philipps-Universität, Hans-Meerwein-Straße, D-35032 Marburg, Germany

E-mail: pitzer@atom.uni-frankfurt.de

Received 3 September 2016, revised 10 October 2016
Accepted for publication 19 October 2016
Published 11 November 2016

Abstract

X-ray single-photon ionization and fragmentation of the chiral molecule halothane from a racemic mixture have been investigated using the cold target recoil ion momentum spectroscopy technique. Two important facets related to the core ionization of this species are examined: Firstly, the distinction of enantiomers (mirror isomers) and the determination of absolute configuration on a single-molecule level by four-body Coulomb explosion; secondly, the interplay of site-selective excitation and fragmentation patterns. These results are easily transferable to other molecular species and show the wealth of features that can be investigated by coincidence spectroscopy of chiral molecules.

Keywords: coulomb explosion imaging, chirality, absolute configuration, photoionization, synchrotron, core excitation, cold target recoil ion momentum spectroscopy (COLTRIMS)

(Some figures may appear in colour only in the online journal)

1. Introduction

Symmetries are one of the most intriguing phenomena for the human spirit, be it in arts, in music or as a principle in our description of nature. Especially in physics, it had been assumed since the days of Isaac Newton that space and time were symmetric, i.e. that a space–time inversion of a closed physical system would not change its intrinsic interactions and dynamics. It was the discovery of the parity violation, first theoretically by Lee and Yang [1] and immediately afterwards by the experiment of Wu and co-workers [2] that put an end to this presumed certainty.

From the point of view of a chemist, and especially a biochemist and molecular biologist, the preponderance of a certain spatial direction or spatial configuration is a fact known since the middle of the 19th century. At that time, molecular chirality was discovered, i.e. the fact that certain molecules occur in two mirror image structures. For most chiral species, one of these so-called enantiomers was found in large excess in living nature, a circumstance known as biomolecular homochirality.

After the discovery of parity violation, hypotheses to link this fundamental asymmetry to biomolecular homochirality quickly arose. These hypotheses can be categorized into two main lines of thought: on the one hand, parity violation introduces a small difference in the energy levels of the two enantiomers [3]. On the other hand, the asymmetry of the weak-interaction-induced β-decay could have favored one enantiomer over the other (Vester–Ulbricht hypothesis) [4].

[5] This article belongs to the special issue: emerging leaders, which features invited work from the best early-career researchers working within the scope of *J. Phys. B*. This project is part of the Journal of Physics series' 50th anniversary celebrations in 2017. Martin Pitzer was selected by the Editorial Board of *J. Phys. B* as an Emerging Leader.

So far, none of these explanations have been able to establish an unequivocal link between the fundamental parity violation and the biomolecular homochirality on Earth. Many calculations and great experimental efforts have been devoted to the parity violating energy difference $\Delta_{PV}E$, but due to the extreme weakness of the effect (the expected relative shift of spectral lines $\Delta_{PV}E/(h\nu)$ being typically below 10^{-13} for experimentally accessible species [5, 6]), no observation has been successful so far. Some authors concluded that the parity violation of the weak interaction is entirely independent from the one observed on the biological level [7], but the question of a possible causal connection between fundamental parity-violation and biomolecular homochirality is still to be regarded as open [3, 8].

The investigation of chiral molecules is not only of fundamental but also of practical interest. It has been reported for various pharmaceutical substances that only one of the enantiomers is of therapeutic use (e.g. ethambutol [9]) or that the wrong enantiomer is even toxic (e.g. penicillamine [10]). Much effort has been devoted to developing enantiopure substances [11] and a wealth of techniques have been developed to distinguish and separate the enantiomers of a given species (see. e.g. [12]).

Even though these techniques are well established, they do not yield direct information on the handedness of the molecular structure under investigation because only a macroscopic effect is measured. Accordingly, a particularly intriguing question is left open: Which sign of the observed effect is correlated to which of the two possible microscopic structures? This issue is known as the problem of absolute configuration. The sign of a macroscopic effect, usually the optical rotation at the sodium D-line ($\lambda = 589$ nm), leads to the designation of enantiomers by $(+)/(-)$, whereas the nomenclature rules coined by Cahn, Ingold and Prelog [13] allow to assign the labels 'right-handed' (*R*) or 'left-handed' (*S*) to the molecular structure models. The link between measured macroscopic effect and corresponding microscopic arrangement is in indirect methods provided by theoretical models or semi-empirical rules. A direct determination of the absolute configuration of the underlying microscopic structure has only been possible with techniques based on anomalous x-ray diffraction as introduced by Bijvoet *et al* [14].

Chiral molecules have increasingly attracted attention in the physics community in the last two decades because gas-phase techniques have been developed that allow to study isolated chiral molecules. Under these circumstances, solvent and collective effects can be neglected and a deeper understanding of the molecules themselves and their light–matter interaction is possible. A list of major techniques encompasses photoelectron circular dichroism (PECD) [15], microwave spectroscopy [16], and several mass-spectroscopic methods [17, 18].

A new prospect for investigating the relation between structure and dynamics was opened recently when coincidence experiments successfully showed that the enantiomers of simple chiral species could be distinguished on the level of individual molecules [19]. These measurements employed so-called coulomb explosion imaging (CEI) [20] to gain information on the molecular configuration. When multiple ionization of a molecule occurs on a timescale shorter than the nuclear motion, the mutual repulsion of the fragment ions can be approximated by the Coulomb interaction. This, in turn, implies that their momentum directions are correlated to the relative positions at the time of ionization. In the measurements mentioned above, a femtosecond laser pulse was employed to multiply ionize the chiral prototype CHBrClF; the momentum vectors of all five atomic cations were measured in coincidence. These momentum vectors yielded a clearly separated signal from the two enantiomers. An experiment using foil-induced CEI was able to determine the absolute configuration for a non-racemic sample of a deuterated chiral epoxide [21].

Similar coincidence techniques have been employed to determine the absolute configuration of laser-aligned molecules [22] and to investigate photoelectron circular dichroism for specific ionic fragments [23]. The coincident measurement of electron and ion momenta allows to define new observables that are sensitive to symmetry violations and to the role of electron dynamics for molecular properties [24].

Recently, it has been demonstrated that Coulomb explosion of a chiral species can efficiently be induced by core ionization with an x-ray photon from a synchrotron source [25]. There, the distinction of enantiomers is even superior to the results obtained with a femtosecond laser. This is attributed to the shorter time-scale of the multiple ionization: the electronic processes after core excitation (e.g. Auger cascades) are expected to be faster (a few fs) than the usual pulse duration of a femtosecond laser pulse (around 40 fs).

In this work we extend our method to a slightly more complex molecule, the chiral ethane derivative halothane $CHBrClCF_3$. It is supposed that (+)-halothane has (*S*)-configuration [26]. World Health Organization's *Model Lists of Essential Medicines* includes halothane [27], although its use is decreasing due to its hepatotoxicity. Concerning stereospecific effects, a study reports slightly different physiological effects of the enantiomers [28]. Inner shell photoionization and subsequent fragmentation have been investigated by Souza *et al* [29]. Halothane showcases two aspects that become relevant when extending CEI to larger molecules: can the configuration be determined again on a single-molecule level for a molecule that consists not only of a single carbon center? How does the fragmentation dynamics change depending on which carbon atom is initially excited and can we use this to enhance relevant fragmentation channels for the determination of absolute configuration?

Concerning the first question, results from our previous experiments show that molecular fragments (in contrast to atomic ions) can also be used for the determination of absolute configuration [25]. A similar approach has been employed, for example, to extract the photodynamics of deuterated benzene from the momentum correlations of molecular fragments [30].

The second aspect, the interplay between selective excitation and fragmentation pathways has been investigated since the early days of synchrotron radiation and electron–ion

coincidence spectroscopy [31]. Particularly interesting for the investigation of halothane is the observation by Habenicht *et al* [32] that the yield of CF_3^+ from trifluoroethane (CF_3CH_3) increases significantly for excitation of the 'opposite' carbon atom C_H. More recent experiments employ photoelectron–photoion–photoion-coincidence-spectra (PEPIPICO), e.g. to investigate the conditions for which site-specific fragmentation works best [33].

2. Methods

The experiments were performed with a cold target recoil ion momentum spectroscopy-setup (COLTRIMS, [34, 35]). Molecules from a supersonic gas jet are crossed orthogonal with ionizing radiation; the resulting fragments (cations and electrons) are projected by an electrostatic field onto time and position sensitive detectors. From the respective times-of-flight and the impact positions on the detector, the momentum vectors of all fragments can be determined in coincidence. As all position and time-of-flight information is stored event by event, possible correlations between fragments can be explored in the offline analysis.

For the results presented here, x-ray photons were used, provided by the beamline SEXTANTS at the synchrotron SOLEIL (Gif-sur-Yvette, France) [36]. The synchrotron was used in timing mode in order to obtain a starting time for the time-of-flight measurements. Several measurements with photon energies between 286 and 305 eV were performed, with energy resolutions ranging from 80 to 300 meV depending on the chosen size of the monochromator exit slits.

The molecular jet was created by expanding halothane in the gas phase through a 200 μm nozzle. The pressure before the nozzle was regulated by a needle valve to a value of 50 mbar which is significantly lower than the vapor pressure of halothane at room temperature (300 mbar). The sample was purchased from Sigma-Aldrich as a racemate (a mixture containing equal amounts of the two enantiomers) and used without further treatment. Before entering the interaction zone, the jet was collimated by two skimmers (0.3 mm diameter each). A gas recycling system with cold traps in the vacuum foreline was used to reduce sample consumption.

In most COLTRIMS-experiments, the electrostatic field in the spectrometer is very low (a few $V\,cm^{-1}$) in order to obtain good momentum resolution. Additionally, the ion arm of the COLTRIMS analyzer is typically very short in order to observe all fragments from a Coulomb explosion with 4π solid angle [37]. This, however, entails a large overlap in the time-of-flight regions of different ion masses. When all fragment ions are detected in coincidence, the correct masses can nevertheless be assigned by checking if the calculated momenta of all the fragments add up to zero.

The more complex a molecule is, the higher the probability that the fragmentation produces neutral fragments which our detector is blind to. This implies that the total momentum of the measured ions does not add up to zero and thus prevents the unambiguous identification of the charged fragments as well. This is especially relevant for the case of missing hydrogen atoms.

To overcome this problem, a new spectrometer was designed using SIMION to simulate the electron and ion trajectories. On the ion side, a higher electric field and a long homogeneous electric field region, together with an electrostatic lens, proved to best fulfill the requirements. An additional field-free drift region was added in front of the ion detector, resembling a spectrometer design which is (employing low electric fields) typically used for investigation of atomic targets. This field design led to a significant improvement in the fragment identification of methyloxirane [38].

An additional benefit of this design is the fact that the ions are accelerated to an energy of around 2000 eV, at which the efficiency of the microchannel-plate detectors already reaches reasonable values. This allows to omit the electrostatic meshes that are usually added in front of the detector to provide a short post-acceleration region with high electric field. As the typical transmission of the employed meshes is 0.78, they lead to a reduction in efficiency by a factor of 2.7 when attempting to measure four particles in coincidence.

The electron side of the spectrometer consisted simply of a homogeneous electric field. The high field that was determined by the ion side of the spectrometer enabled a 4π solid angle for electrons up to a kinetic energy of 35 eV. For this reason, no magnetic field was needed to confine the electron trajectories within the spectrometer. One drawback of this configuration is the reduced time-of-flight spread of the electrons, and in conjunction a poor momentum resolution along the spectrometer axis. For low-energy electrons, the good momentum resolution in the detector plane ($\Delta p \approx 0.01$ atomic units) still allows the precise determination of the electron energy and the investigation of forward-backward asymmetries in the detector plane, i.e. along the photon propagation direction. High-energy electrons, however, have a smaller acceptance angle and are mostly recorded with momenta along the spectrometer axis where the uncertainty is around 0.4 atomic units of momentum. In the case of 80 eV electrons, this leads to an experimental broadening of about 25 eV.

3. Results and discussion

3.1. Determination of configuration and distinction of enantiomers

Similar to the previous experiments, the focus was first on fragmentation pathways without neutral dissociation products. In this case, at least four ions need to be detected to distinguish enantiomers and to determine the absolute configuration. For halothane in the given photon energy range, the break-up into the four ions CH^+, Cl^+, Br^+, and CF_3^+ was the only one that fulfilled all of the above criteria. This fragmentation pathway corresponds to one of the pathways identified for CHBrClF [25], with a CF_3^+ fragment instead of a single F^+ ion. The break-up into the five ions H^+, C^+, Cl^+,

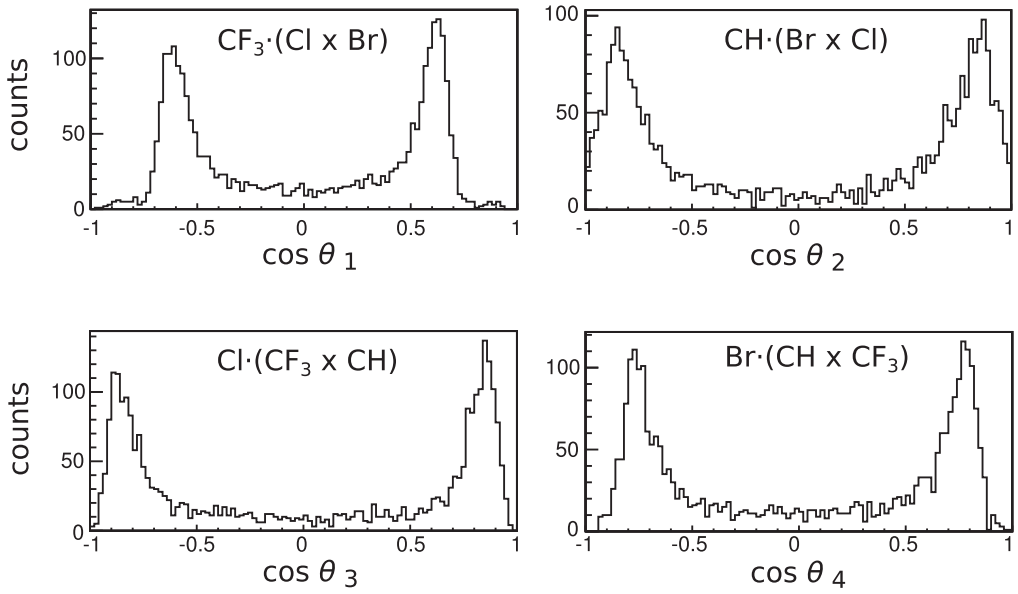

Figure 1. Separation of enantiomers using the chirality parameters $\cos(\theta_i)$ (see text for definition) for the break-up into $\{CH^+, {}^{35}Cl^+, {}^{79}Br^+, CF_3^+\}$, obtained at a photon energy of 305 eV. The two peaks indicate a good separation of enantiomers for each combination of fragments, despite a number of ambiguous events close to $\cos(\theta_i) = 0$. The left peak always corresponds to the *S*-enantiomer, the right one to the *R*-enantiomer.

Br^+, and CF_3^+ was found with such small yield that the separation of peaks for the enantiomers could not be considered statistically significant (for each isotopic combination at a given photon energy around 100 events in total or 15 events per hour of measurement). Figure 1 shows the chirality parameters

$$\cos(\theta_1) = \vec{p}_{CF_3} \cdot (\vec{p}_{Cl} \times \vec{p}_{Br})(|\vec{p}_{CF_3}||\vec{p}_{Cl} \times \vec{p}_{Br}|)^{-1} \equiv CF_3 \cdot (Cl \times Br)$$

etc. The order of fragments is chosen in a way that a value of $\cos(\theta) > 0$ corresponds to an *R*-type configuration of momenta, $\cos(\theta) < 0$ to an *S*-type configuration. In order to relate this configuration to the one of the structure model, it has to be assumed that fragmentation takes place before a stereomutation occurs. To which degree this hypothesis holds, needs to be tested by future measurement with a non-racemic sample. Imposing conditions on the kinetic energy release (KER) of the fragmentation might be necessary to select 'direct' break-up events. Despite a significant number of events in between, the two peaks for the enantiomers can clearly be separated for any combination of three fragments. It should be noted, however, that the different $\cos(\theta_i)$ are not independent from each other because the four momentum vectors nearly add up to zero so that only three linearly independent momentum vectors exist in the system.

The origin of the events close to $\cos(\theta_i) = 0$ remains unclear. One possible explanation is a fragmentation behavior that differs from the supposed 'instantaneous' Coulomb repulsion of the ions. Another reason could be falsely assigned masses, leading to erroneous momentum values; especially events where a single C^+ instead of a CH^+ is detected, could contaminate the depicted distributions. Random coincidences (i.e. ions coming from different molecules) and detector artifacts are expected to play a minor role as the experimental settings were similar to previous measurements [25] where much less ambiguous events were found.

The three-dimensional representation (figure 2) confirms the separation of enantiomers, with the ambiguous events clearly visible (marked by the gray ellipse). In this figure, momentum data (small spheres) are overlaid with a structural model of the *R*- and *S*-enantiomer respectively. The transformation of the data into the molecular frame is chosen in a way that the CH^+ points away from the spectator, defining the first axis of the molecular coordinate systems. The second axis of the molecular coordinate system is defined by the sum momentum of Cl^+ and Br^+.

Information on the absolute configuration can also be obtained from fragmentation pathways involving neutral dissociation products, as long as suitable ionic fragments are detected [25]. For these 'incomplete' break-ups, the assignment of masses becomes ambiguous: first, the isotopes of chlorine and bromine can no longer be separated; second, a contribution from C^+ ions contaminates the CH^+ data. Due to the high field used in the setup, the wrong mass assignment leads to errors of around 100 atomic units (a.u.) in the momenta of the measured ions which severely affects the distinction of enantiomers. In the case of $\{CH^+, Cl^+, Br^+, CF_2^+\}$, the missing fluorine atom carries only a small momentum, leading to an average sum momentum of the detected ions of around 50 atomic units. This still allows us to apply a rather narrow constraint on the sum momentum. Thus, the contribution of the different isotopes can be separated; a clear distinction between enantiomers, however, was only visible when a restriction on the momenta of the individual ions was imposed. The maximum momentum observed in the completely detected break-up (300 atomic units) was taken as upper threshold for the momenta of the individual ions.

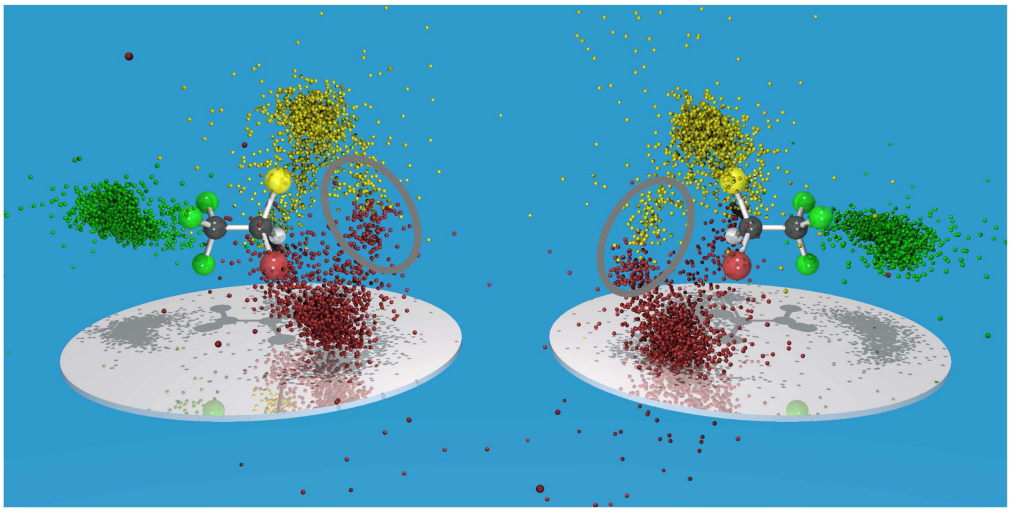

Figure 2. Three-dimensional representation of the data from figure 1, overlaid with a structural model of the (*S*)-enantiomer (left) and (*R*)-enantiomer (right). The color code for the model/the data is as follows: green for F/CF_3^+, yellow for Cl/Cl^+, red for Br/Br^+, black for C/CH^+ and white for H. The momenta of CH^+ constitute one axis of the molecular coordinate system, and are represented by an arrow pointing away from the spectator. Ambiguous events are marked with an ellipse; additional outliers are also visible.

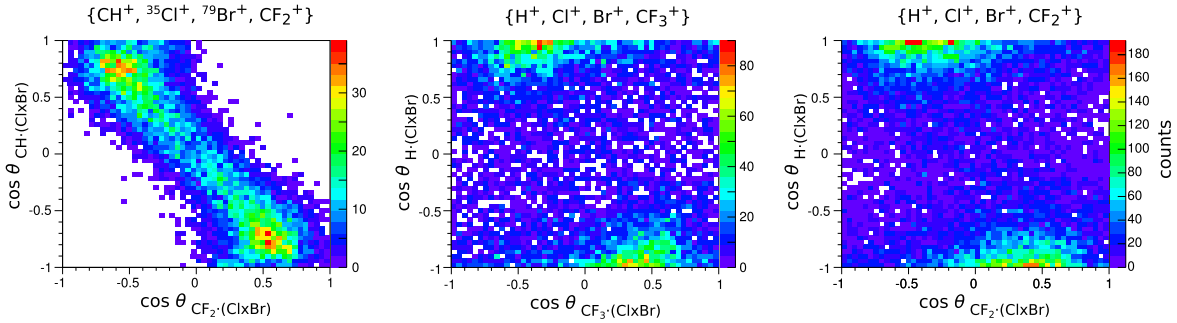

Figure 3. Separation of enantiomers for additional fragmentation pathways, using the angles between ion momenta analogous to figure 1. The ionizing photon energy was 305 eV as well. The break-up into $\{CH^+, {}^{35}Cl^+, {}^{79}Br^+, CF_2^+\}$ (left), $\{H^+, Cl^+, Br^+, CF_3^+\}$ (middle), and $\{H^+, Cl^+, Br^+, CF_2^+\}$ (right) can provide a distinction between enantiomers. For the latter two break-ups, the chlorine and bromine isotopes could not be identified (see text).

Figure 3 (left) shows a two-dimensional representation of the chirality parameters as defined before (with $CF_3 \cdot (Cl \times Br)$ being the shorthand notation for $\vec{p}_{CF_3} \cdot (\vec{p}_{Cl} \times \vec{p}_{Br})(|\vec{p}_{CF_3}||\vec{p}_{Cl} \times \vec{p}_{Br}|)^{-1}$ etc.). Due to the momentum of the undetected fragment, four linearly independent vectors exist for this break-up. This means that, contrary to the previous case, two independent chirality parameters exist which can be plotted against each other. Two peaks for the two enantiomers are visible; their location in the second and fourth quadrant confirms the consistency of enantiomer assignment.

The same condition for the ions' momenta was set for investigating the break-ups $\{H^+, Cl^+, Br^+, CF_3^+\}$ and $\{H^+, Cl^+, Br^+, CF_2^+\}$, i.e. two additional Coulomb explosion pathways that are expected to yield information on the absolute configuration. In this case, a separation of the chlorine and bromine isotopes was not possible anymore. To obtain the momenta from the measured data, a mass of 35 amu was assumed for chlorine (as this isotope has a natural abundance of around 76%) and a mass of 80 amu for bromine (as ^{79}Br and ^{81}Br occur in almost equal amounts). Again two peaks are visible, but at slightly different positions than before: along the *x*-axis, the peaks are close to zero, indicating that the CF_n^+ fragment almost lies in a plane with the chlorine and bromine ion. The proton H^+ is ejected mostly perpendicular to this plane.

The procedure of applying constraints on the individual momenta should be employed with care as it might eliminate not only wrong mass assignments but also possible break-ups with different dynamics. In future experiments on isotope-containing species, the spectrometer design should be adjusted according to these findings.

For possible future applications, the precision in the determination of the enantiomeric excess $ee = (R - S)/(R + S)$, with *R* and *S* being the numbers of right- and left-handed molecules respectively, is of great interest. If no background was present, the precision would only be limited by the statistic uncertainty in the number of counts for the two enantiomers. In the case of the complete break-up $\{CH^+, Cl^+, Br^+, \text{and } CF_3^+\}$ a simple background subtraction was performed by taking only events with $|\cos(\theta_1)| > 0.4$. From

Table 1. Yield of different four-body fragmentation pathways normalized to the total number of events. The relative yield of the first two pathways does not change when going above the carbon 1s ionization threshold. The fragmentation pathways with a detected proton are slightly enhanced when C_F can be photoionized (bold font).

Detected fragments	Photon energy		
	305.0 eV	299.0 eV	286.9 eV
$\{CH^+, CF_3^+, Cl^+, Br^+\}$	3.9×10^{-5}	2.7×10^{-5}	4.7×10^{-5}
$\{CH^+, CF_2^+, Cl^+, Br^+\}$	1.8×10^{-4}	1.2×10^{-4}	2.1×10^{-4}
$\{H^+, CF_3^+, Cl^+, Br^+\}$	$\mathbf{1.2 \times 10^{-4}}$	3.4×10^{-5}	3.2×10^{-5}
$\{H^+, CF_2^+, Cl^+, Br^+\}$	$\mathbf{2.8 \times 10^{-4}}$	2.9×10^{-5}	6.4×10^{-5}

Table 2. Yield of different two-body fragmentation pathways, again normalized to the total number of events. For the first two break-ups, the relative yield is smaller above the carbon 1s threshold than below. This indicates that—contrary to the integral ionization probability—their probabilities are not increasing above the carbon 1s threshold.

Detected fragments	Photon energy		
	305.0 eV	299.0 eV	286.9 eV
$\{Br^+, CHClCF_3^+\}$ (**I**)	2.3×10^{-4}	1.8×10^{-4}	3.2×10^{-4}
$\{Cl^+, CHBrCF_3^+\}$ (**II**)	1.3×10^{-4}	1.0×10^{-4}	2.4×10^{-4}
$\{CF_3^+, CHClBr^+\}$ (**III**)	8.3×10^{-5}	7.9×10^{-5}	7.2×10^{-5}

these events, an enantiomeric excess of $ee = (0.1 \pm 1.3)\%$ was deduced, confirming the racemic nature of the sample.

3.2. Site-selective excitation

Most chiral molecules contain several carbon atoms. This raises the question if selective excitation at the stereocenter can be used to preferentially break its bonds and to yield fragments that allow determination of absolute configuration. In halothane, the inner shells of the carbon in the CF_3 group (we will denote this carbon as C_F in the following) are expected to have a larger binding energy than the corresponding levels of the stereocenter $C^\star$. This is due to the higher electronegativity of fluorine compared to bromine, chlorine and hydrogen.

A scan over a photon energy range from 280 to 305 eV was performed, recording the total ion yield and the yield of CF_3^+ ions. As the features could not unambiguously be assigned to resonant excitations of one of the carbon atoms, the following photon energies were chosen: 286.9 eV (below excitation of the carbon atoms), 299.0 eV (photoionization of the stereocenter only) and 305.0 eV (photoionization of both carbon atoms). For the latter two energies, the coincident measurement of the electron energy allows us to determine the excitation site. The first one was chosen to evaluate the influence of excitation from different halogen shells that have previously been found to play a role in the multiple ionization [25].

Confirming our previous work [25], the electron energy spectra for the fragmentation into four cations do not show any structures. This could be due to the physical processes leading to this fragmentation or due to experimental limitations that do not allow to detect four electrons in coincidence correctly. An effect of site-specific excitation, if any, can thus only be found in the relative abundance of the different fragmentation pathways. Table 1 shows the yield of the four fragmentation pathways discussed in the previous section, normalized to the total number of events, for the different photon energies. This quantity appears most suitable for normalization as the density of the molecular jet and the photon flux were slightly different for the different measurements.

The first two break-ups, involving a CH^+ ion do not show significant dependence of the photon energy. The break-ups where a proton was detected seem to have a higher yield by a factor of 3 when the photon energy is above the ionization threshold of C_F. As the yield of the $\{H^+, CF_2^+, Cl^+, Br^+\}$ does not show a clear tendency, the numbers shown do not provide a watertight indication of selective excitation. In addition, an increase is expected above the photoionization threshold of the stereocenter (i.e. at 299 eV in our experiment), as the hydrogen is bound to $C^\star$.

We therefore chose to additionally investigate the selective excitation for fragmentation into two cations where clear features in the electron spectra can be seen. Three break-ups could be identified that are 'complete', i.e. where the sum of fragment masses corresponds to the parent ion's mass: $\{Br^+, CHClCF_3^+\}$ (**I**), $\{Cl^+, CHBrCF_3^+\}$ (**II**), and $\{CF_3^+, CHClBr^+\}$ (**III**).

Table 2 contains the relative yields of these three channels, again normalized to the total number of events for the reasons stated before. When looking at the numbers, it has to be taken into account that more ionization pathways are energetically accessible above the respective 1s thresholds of the two carbon atoms. The low relative yield of pathways **I** and **II** at a photon energy of 305 eV is thus attributed to the fact that these two pathways are independent of the carbon 1s ionization.

This hypothesis is confirmed by looking at the electron spectra. Figure 4 shows the energy spectra for different photon energies (rows) and fragmentation pathways (columns).

Pathway **I**: when a bromine ion is split from the molecule, the corresponding electron spectrum shows a peak at around 45 eV. As this peak does not shift with the excitation energy, it is attributed to an Auger decay. The peak position and width correspond to the electron energy distribution discussed in [39] and attributed there to valence–valence Auger processes after the bromine 3d excitation. Surprisingly, no photoelectron was found in this break-up channel for any of the exciting energies. This could be due to the fact that the solid angle for electrons with an energy above 200 eV (the bromine 3d level being at 81 eV) was very small. Additionally, an electron of a kinetic energy of 200 eV is detected with a resolution of 45 eV and thus dramatically smeared out in the spectrum.

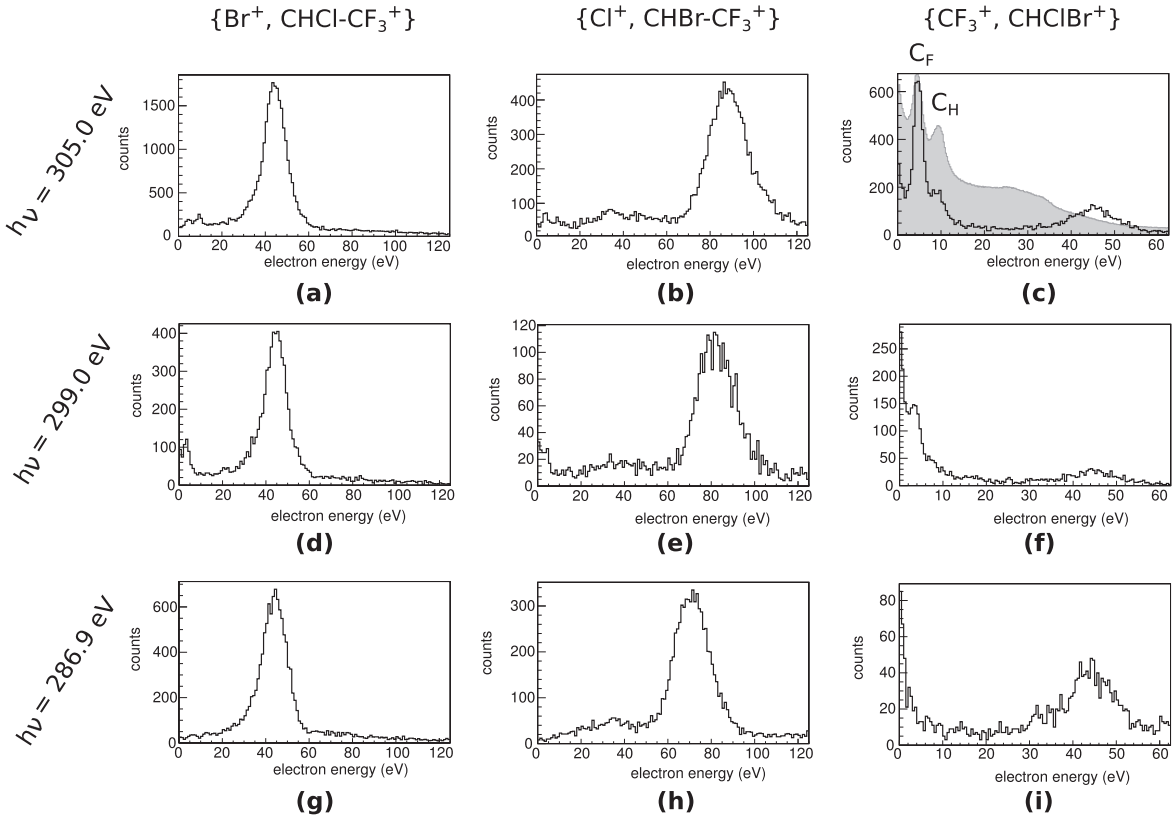

Figure 4. Electron energy spectra for three different fragmentation pathways (columns) and different photon energies (rows). The constant electron energy in the left column indicates that an Auger process is dominant for the split-off of a bromine cation. In the case of the chlorine cation (center column), the shift reveals a photoelectron that can be attributed to the chlorine 2p shell. In the case of the rather symmetric break-up with a CF_3^+ detached (right column), the low-energy photoelectron indicates excitation of the carbon 1s shell. Comparison with an integral electron spectrum (shaded in figure (c)) indicates that most ionization is from C_F. A different energy range and a different binning were chosen for the right column.

Pathway **II**: in the case of a separated chlorine ion, a peak is observed in the spectrum that shifts roughly with the photon energy. In this case, the experimental broadening discussed in the experimental section plays a significant role. Although a precise determination of the energy is not possible, the attribution as a photoelectron from the chlorine 2p level (206.8 eV for the atomic species [40]) seems justified.

Pathway **III**: only the break-up involving CF_3^+ is clearly connected to the excitation of the C 1s shell: for the highest photon energy, a distinct peak is observed that corresponds to the lower electron energy in the integral electron spectrum (shaded area), together with a shoulder at the higher electron energy. This indicates that the break-up is preferentially induced by excitation of the 1s shell of C_F. The spectra at $h\nu = 299.0$ eV and $h\nu = 286.9$ eV support this finding. In the former one, the strong peak has disappeared, in the latter one, no sign of a photoelectron is visible. The relatively high yield at 299.0 eV might be due to the fact that the energy is very close to the threshold of C_F. These results show that a specific fragmentation pathway can strongly correlate to the selective excitation of one carbon atom.

In the case of halothane, various shells from the halogen atoms contribute to the ionization, thus preventing a truly selective excitation. At the photon energies used, the cross sections for photoionization from the chlorine 2p and the bromine 3d level are even higher than for the targeted carbon 1s. For oxygen and nitrogen, in contrast, the photoionization cross section at 300 eV is more than an order of magnitude lower than for carbon [40]. The probability for alternative ionization pathways is thus expected to decrease significantly for organic species that contain only oxygen or nitrogen in addition to carbon and hydrogen. The crucial question in this case will be if the levels of the carbon atoms differ enough to enable a selective excitation.

4. Conclusion

The chiral ethane derivative halothane was investigated using x-ray photons for core ionization and a COLTRIMS-setup for coincident detection of the fragments. A separated signal of the enantiomers—assuming instantaneous multifragmentation—could be found in several four-body Coulomb explosion pathways. The CF_3^+ cation is an example of a complete functional group that was used to determine absolute configuration. This finding is an encouraging step towards application of the method to biologically relevant molecules. Due to multiple possible fragmentation pathways the yield of chirality-sensitive pathways was very low. Nevertheless, the

racemic nature of the sample was confirmed with an error of about 1%.

The site-selective excitation of the two carbon atoms was investigated for four-body fragmentations and in the case of double ionization, leading to two-body fragmentation. Two of the four-body fragmentation pathways show an increase for photon energies where both carbon atoms can be photo-ionized. In the case of two-particle break-ups, the splitting of the CF_3^+ from the rest of the molecule clearly correlates with excitation of the C_F. For other break-ups, the contribution of chlorine and bromine shells is dominant, providing rather element-selectivity than a site-selectivity.

The results presented here show that coincidence measurements can yield information on the absolute configuration of molecules containing more than one carbon atom. These results are a further step towards analytical applications of the method and provide a good example for linking site-selective excitation with investigations of molecular structure.

Acknowledgments

We thank the staff of the synchrotron SOLEIL, in particular Nicolas Jaouen from beamline SEXTANTS for their outstanding support. Markus Schöffler acknowledges support by the Adolf Messer foundation. This work was supported by the State Initiative for the Development of Scientific and Economic Excellence (LOEWE) in the LOEWE-Focus ELCH.

References

[1] Lee T D and Yang C N 1956 Question of parity conservation in weak interactions *Phys. Rev.* **104** 254–8
[2] Wu C S, Ambler E, Hayward R W, Hoppes D D and Hudson R P 1957 Experimental test of parity conservation in beta decay *Phys. Rev.* **105** 1413–5
[3] Quack M 2002 How important is parity violation for molecular and biomolecular chirality? *Ang. Chem., Int. Ed.* **41** 4618–30
[4] Vester F, Ulbricht T L V and Krauch H 1959 Optische Aktivität und die paritätsverletzung im β-zerfall *Die Naturwissenschaften* **46** 68
[5] Darquié B *et al* 2010 Progress toward the first observation of parity violation in chiral molecules by high-resolution laser spectroscopy *Chirality* **22** 870–84
[6] Berger R 2004 Parity violation effects in molecules *Relativistic Electronic Structure Theory: II. Applications* ed P Schwerdtfeger (Amsterdam: Elsevier) pp 188–288
[7] Bonner W A 2000 Parity violation and the evolution of biomolecular homochirality *Chirality* **12** 114–26
[8] Berger R and Quack M 2000 Electroweak quantum chemistry of alanine: parity violation in gas and condensed phases *Chem. Phys. Chem.* **1** 57–60
[9] Wilkinson R G, Shepherd R G, Thomas J P and Baughn C 1961 Stereospecificity in a new type of synthetic antituberculous agent *J. Am. Chem. Soc.* **83** 2212
[10] Walshe J M 1992 Chirality of penicillamine *Lancet* **339** 254
[11] McConnell O *et al* 2007 Enantiomeric separation and determination of absolute stereochemistry of asymmetric molecules in drug discovery—building chiral technology toolboxes *Chirality* **19** 658–82
[12] Wolf C 2007 *Dynamic Stereochemistry of Chiral Compounds: Principles and Applications* 1st edn (Cambridge: Royal Society of Chemistry)
[13] Cahn R S and Ingold C K 1951 Specification of configuration about quadricovalent asymmetric atoms *J. Chem. Soc.* 612–22
[14] Bijvoet J M, Peerdeman A F and van Bommel A J 1951 Determination of the absolute configuration of optically active compounds by means of x-rays *Nature* **168** 271–2
[15] Janssen M H M and Powis I 2014 Detecting chirality in molecules by imaging photoelectron circular dichroism *Phys. Chem. Chem. Phys.* **16** 856–71
[16] Patterson M, Schnell M and Doyle J M 2013 Enantiomer-specific detection of chiral molecules via microwave spectroscopy *Nature* **497** 475–8
[17] Horsch P, Urbasch G, Weitzel K-M and Kröner D 2011 Circular dichroism in ion yields employing femtosecond laser ionization—the role of laser pulse duration *Phys. Chem. Chem. Phys.* **13** 2378–86
[18] Zehnacker A (ed) 2010 *Chiral Recognition in the Gas Phase* (London: Taylor and Francis)
[19] Pitzer M *et al* 2013 Direct determination of absolute molecular stereochemistry in gas phase by coulomb explosion imaging *Science* **413** 1096–100
[20] Vager Z, Naaman R and Kanter E P 1989 Coulomb explosion imaging of small molecules *Science* **244** 426–31
[21] Herwig P *et al* 2013 Imaging the absolute configuration of a chiral epoxide in the gas phase *Science* **342** 1084–6
[22] Christensen L, Nielsen J H, Slater C S, Lauer A, Brouard M and Stapelfeldt H 2015 Using laser-induced coulomb explosion of aligned chiral molecules to determine their absolute configuration *Phys. Rev.* A **92** 033411
[23] Fanood M M R, Ram N B, Lehmann C S, Powis I and Janssen M H M 2015 Enantiomer-specific analysis of multi-component mixtures by correlated electron imaging-ion mass spectrometry *Nat. Commun.* **6** 7511
[24] Trinter F *et al* 2012 Multi-fragment vector correlation imaging. a search for hidden dynamical symmetries in many-particle molecular fragmentation processes *Mol. Phys.* **110** 1863–72
[25] Pitzer M *et al* 2016 Absolute configuration from different multifragmentation pathways in light-induced coulomb explosion imaging *Chem. Phys. Chem.* **17** 2465–72
[26] Ramig K, Lavinda O and Szalda D J 2012 The highly stereoselective decarboxylation of (+)-1-bromo-1-chloro-2-trifluoropropanoic acid to give (+)-1-bromo-1-chloro-2-trifluoroethane [(+)-halothane] with retention of configuration *Tetrahedron* **23** 201–4
[27] World Health Organization WHO Model Lists of Essential Medicines (http://who.int/medicines/publications/essentialmedicines/en/)
[28] Harris B D, Moody E J and Skolnick P 1998 Stereoselective actions of halothane at $GABA_A$ receptors *Eur. J. Pharm.* **341** 349–52
[29] de Souza G G B, dos Santos A C F, Rocco M L M, Lucas C A, Boechat-Roberty H M and de Brito A N 2001 Fragmentation of molecules by synchrotron radiation and by fast electrons: I. The case of halothane, C_2F_3HClBr *Quim. Nova.* **24** 311–4
[30] Matsuda A, Fushitani M, Thomas R D, Zhaunerchyk V and Hishikawa A 2009 Multiple explosion pathways of the deuterated benzene trication in 9-fs intense laser fields *J. Phys. Chem.* A **113** 2254–60
[31] Eberhardt W, Sham T K, Carr R, Krummacher S, Strongin M, Wenig S L and Wesner D 1983 Site-specific fragmentation of small molecules following soft-x-ray excitation *Phys. Rev. Lett.* **50** 1038–41
[32] Habenicht W, Baiter H, Müller-Dethlefs K and Schlag E W 1991 Memory effects in molecular fragmentation induced by site-specific core excitation using a reflectron time-of-flight mass spectrometer *J. Phys. Chem.* **95** 6774–80

[33] Nagaoka S *et al* 2011 A study to control chemical reactions using Si:2p core ionization: site-specific fragmentation *J. Phys. Chem.* A **115** 8822–31
[34] Dörner R, Mergel V, Jagutzki O, Spielberger L, Ullrich J, Moshammer R and Schmidt-Böcking H 2000 Cold target recoil ion momentum spectroscopy: a momentum microscope to view atomic collision dynamics *Phys. Rep.* **330** 95–192
[35] Ullrich J, Moshammer R, Dorn A, Dörner R, Schmidt L P H and Schmidt-Böcking H 2003 Recoil-ion and electron momentum spectroscopy: reaction-microscopes *Rep. Prog. Phys.* **66** 1463–545
[36] Sacchi M *et al* 2013 The SEXTANTS beamline at SOLEIL: a new facility for elastic, inelastic and coherent scattering of soft x-rays *J. Phys.: Conf. Ser.* **425** 072018
[37] Jahnke T, Weber T, Osipov T, Landers A L, Jagutzki O, Schmidt L P H, Cocke C L, Prior M H, Schmidt-Böcking H and Dörner R 2004 Multicoincidence studies of photo and Auger electrons from fixed-in-space molecules using the COLTRIMS technique *J. Elec. Spect.* **141** 229–38
[38] Tia M *et al* 2016 Observation of enhanced chiral asymmetries in the inner-shell photoionization of uniaxially oriented methyloxirane enantiomers (arXiv:1609.03828)
[39] Miron C, Simon M, Leclerq N, Hansen D L and Morin P 1998 Site-selective photochemistry of core excited molecules: role of the internal energy *Phys. Rev. Lett.* **81** 4104–7
[40] Yeh J J and Lindau I 1985 Atomic subshell photoionization cross sections and asymmetry parameters: $1 \leqslant Z \leqslant 103$ *At. Data Nucl. Data Tables* **232** 1–55